Novel loss-of-function variants expand *ABCC9*-related intellectual disability and myopathy syndrome

Stephanie Efthymiou,[1,†] Marcello Scala,[1,2,3,†] Vini Nagaraj,[4] Katarzyna Ochenkowska,[5] Fenne L. Komdeur,[6] Robin A. Liang,[7] Mohamed S. Abdel-Hamid,[8] Tipu Sultan,[9] Tuva Barøy,[10] Marijke Van Ghelue,[7] Barbara Vona,[11] Reza Maroofian,[1] Faisal Zafar,[12] Fowzan S. Alkuraya,[13] Maha S. Zaki,[14] Mariasavina Severino,[15] Kingsley C. Duru,[4] Robert C. Tryon,[16] Lin Vigdis Brauteset,[17] Morad Ansari,[18] Mark Hamilton,[19] Mieke M. van Haelst,[6] Gijs van Haaften,[20] Federico Zara,[3] Henry Houlden,[1] Éric Samarut,[5] Colin G. Nichols,[16] Marie F. Smeland[21,22] and Conor McClenaghan[4]

[†]**These authors contributed equally to this work.**

Abstract

Loss-of-function mutation of *ABCC9*, the gene encoding the SUR2 subunit of ATP sensitive-potassium (K_{ATP}) channels, was recently associated with autosomal recessive *ABCC9*-related intellectual disability and myopathy syndrome (AIMS).

Here we identify nine additional subjects, from seven unrelated families, harboring different homozygous LoF variants in *ABCC9* and presenting with a conserved range of clinical features. All variants are predicted to result in severe truncations or in-frame deletions within SUR2, leading to the generation of non-functional SUR2-dependent K_{ATP} channels.

Affected individuals show psychomotor delay and intellectual disability of variable severity, microcephaly, corpus callosum and white matter abnormalities, seizures, spasticity, short stature, muscle fatigability, and weakness. Heterozygous parents do not show any conserved clinical pathology but report multiple incidences of intrauterine fetal death, which were also observed in an eighth family included in this study. *In vivo* studies of abcc9 LoF in zebrafish revealed an exacerbated motor response to pentylenetetrazole, a pro-convulsive drug, consistent with impaired neurodevelopment associated with an increased seizure susceptibility.

Our findings define an *ABCC9* LoF related phenotype, expanding the genotypic and phenotypic spectrum of AIMS and reveal novel human pathologies arising from K_{ATP} channel dysfunction.

Author affiliations:

1 Department of Neuromuscular Disorders, UCL Queen Square Institute of Neurology, University College London, London, WC1N 3BG, UK

2 Department of Neurosciences, Rehabilitation, Ophthalmology, Genetics, Maternal and Child Health, University of Genoa, 16147 Genoa, Italy

3 U.O.C. Genetica Medica, IRCCS Istituto Giannina Gaslini, 16147 Genoa, Italy

4 Center for Advanced Biotechnology and Medicine, and Departments of Pharmacology and Medicine, Robert Wood Johnson Medical School, Rutgers The State University of New Jersey, NJ 08854, USA

5 Centre de Recherche du Centre Hospitalier de l'Université de Montréal (CRCHUM), and Department of Neuroscience, Université de Montréal, Montreal H2X 0A9, Quebec, Canada

6 Section Clinical Genetics, Dept. Human Genetics and Amsterdam Reproduction & Development, Amsterdam University Medical Centers, 1105 AZ Amsterdam, The Netherlands

7 Department of Medical Genetics, Division of Child and Adolescent Health, University Hospital of North Norway, 9019 Tromsø, Norway

8 Medical Molecular Genetics Department, Human Genetics and Genome Research Institute, National Research Centre, Cairo 12622, Egypt

9 Department of Pediatric Neurology, Children Hospital, University of Child Health Sciences, Lahore, Punjab 54000, Pakistan

10 Department of Medical Genetics, Oslo University Hospital, 0450 Oslo, Norway

11 Institute of Human Genetics and Institute for Auditory Neuroscience and InnerEarLab, University Medical Center Göttingen, 37073 Göttingen, Germany

12 Department of Paediatric Neurology, Children's Hospital and Institute of Child Health, Multan, Punjab 60000, Pakistan

13 Department of Translational Genomics, Center for Genomic Medicine, King Faisal Specialist Hospital and Research Center, Riyadh 12713, Saudi Arabia

14 Clinical Genetics Department, Human Genetics and Genome Research Institute, National Research Centre, Cairo 12622, Egypt

15 Neuroradiology Unit, IRCCS Istituto Giannina Gaslini, 16147 Genova, Italy

16 Department of Cell Biology and Physiology, and Center for the Investigation of Membrane Excitability Diseases (CIMED), Washington University, St Louis, MO 63110, USA

17 Division of Habilitation for Children, Innlandet Hospital Sanderud, Hamar, 2312, Norway

18 South East Scotland Genetic Service, Western General Hospital, Edinburgh, EH4 2XU, UK

19 West of Scotland Clinical Genetics Service, Queen Elizabeth University Hospital, Glasgow, G51 4TF, UK

20 Department of Genetics, University Medical Center Utrecht, 3584 CX, The Netherlands

21 Department of Pediatric Rehabilitation, University Hospital of North Norway, 9019 Tromsø, Norway

22 UiT The Arctic University of Norway, 9019 Tromsø, Norway

Correspondence to: Conor McClenaghan

The Center for Advanced Biotechnology and Medicine, Rutgers, The State University of New Jersey, 679 Hoes Lane West, Piscataway, NJ 08854, USA

E-mail: conor.mcclenaghan@rutgers.edu

Correspondence may also be addressed to: Marie Smeland

Department of Pediatric Rehabilitation, University Hospital of North Norway, 9019 Tromsø, Norway

E-mail: marie.smeland@unn.no

Running title: *ABCC9* loss-of-function causes AIMS

Keywords: KATP channels; SUR2; ABCC9; neurodevelopmental disorder

Introduction

ABCC9-related intellectual disability and myopathy syndrome (AIMS; OMIM # 619719) was recently identified in six individuals, from two families, who were all homozygous for the same loss-of-function (LoF) splice-site variant in *ABCC9* (NM_005691: c.1320+1G>A)[1]. *ABCC9* encodes the SUR2 (sulfonylurea receptor 2) subunit of ATP-sensitive potassium (K_{ATP}) channels, which are widely expressed throughout the body. K_{ATP} channels are nucleotide-regulated potassium channels, comprising pore-forming Kir6 subunits co-assembled with regulatory SUR subunits, that couple cellular metabolism and diverse cellular signaling pathways to the membrane potential[2].

The two mammalian Kir6 isoforms, Kir6.1 (*KCNJ8*) and Kir6.2 (*KCNJ11*) and two SUR isoforms, SUR1 (*ABCC8*) and SUR2 (*ABCC9*), show distinct properties and tissue expression patterns. SUR proteins are members of the ABC-transporter family and share core structural features of two transmembrane domains (TMD1 and TMD2) and two nucleotide binding domains (NBD1 and NBD2) with family members such as CFTR (*ABCC7*) and the multidrug resistance protein (MRP-1; *ABCC1*). SURs have no recognized transporter function, but instead, regulate K_{ATP} channel complexes, conferring Mg-nucleotide activation and pharmacological sensitivity, and modulating ATP inhibition[2]. Functional K_{ATP} channel expression at the plasma membrane requires co-assembly of four Kir6 subunits with four SUR subunits[3-9]. Extensive study has shown that truncation of SUR proteins impairs or abolishes surface expression of K_{ATP} channels[10,11], and truncations of SUR1 are associated with congenital hyperinsulinism due to loss of pancreatic K_{ATP} function[12].

SUR2-containing K_{ATP} channels are well described in multiple tissues, including smooth, cardiac and skeletal muscle[13,14]. Channel activity serves to hyperpolarize the membrane potential in smooth muscle, reducing vascular tone, gastrointestinal motility, and lymphatic contractility[15-19]. In striated muscle, channel activation results in action potential shortening in cardiac muscle, and decreased action potential amplitudes and membrane potential hyperpolarization in skeletal

muscle[20-24]. Additional roles for SUR2 containing channels have been proposed in diverse tissues including the brain, bone, hair follicles, fibroblasts, and the endothelia[13,25-29].

The previously reported AIMS individuals displayed cognitive impairment, muscle weakness, fatigability, facial dysmorphism, white matter hyperintensities, and cardiac systolic dysfunction in older individuals. Some of these features, such as the musculoskeletal and cardiac dysfunction, were predicted from earlier studies of K_{ATP} channel gene knockout mice[20,23,24,30-32]. In contrast, cognitive and neurological impairment remains to be explained.

We now report nine new individuals, from seven unrelated families, harboring biallelic variants in *ABCC9* who present with a distinctive neurodevelopmental phenotype consistent with previously reported AIMS patients, and associated with imaging features resembling periventricular leukomalacia and brain calcifications. Each family presents with different *ABCC9* variants that are predicted to result in major deletions or truncations of the SUR2 protein, and which we show lead to complete loss-of-function of recombinant K_{ATP} channels. Novel genotypes associated with phenotypes that are consistent with previously reported AIMS patients, and the identification of additional novel features, expands this *ABCC9* LoF-associated recessive disorder.

Materials and methods

Patients

Written informed consent was obtained from the parents or legal guardians of all enrolled individuals. Patient data were anonymized before sharing. Subjects were recruited from several clinical and research centers in Europe, Africa, the Middle East, and Asia (Department of Human Genetics, Amsterdam University Medical Center, Amsterdam, the Netherlands; University Hospital of North Norway, Tromsø, Norway; UCL Queen Square Institute of Neurology, UK; National Research Centre, Cairo, Egypt; King Abdullah International Medical Research Center, Riyadh, Saudi Arabia; Multan Children's Hospital, Multan, Pakistan, King Faisal Specialist Hospital and Research Center, Riyadh, Saudi Arabia, and West of Scotland Clinical Genetics Service, UK).

Clinical evaluation

Developmental history, behavioral disturbances, neurological examinations, and electro-clinical findings were collected from clinical charts and thoroughly reviewed by the referring physicians and pediatricians with expertise in pediatric neurology. Brain MRIs were performed locally, and neuroimaging findings were systematically reviewed by an expert pediatric neuroradiologist. Molecular and clinical findings of previously reported AIMS patients[1] were reviewed and compared with the current cohort.

Genotyping

Whole exome sequencing (WES) was performed, where indicated, on genomic DNA extracted from peripheral blood leukocytes separately at three different laboratories as previously described[33]. Genetic variants were filtered according to allele frequency ≤ 0.001 in the Genome Aggregation Database (gnomAD; https://gnomad.broadinstitute.org), presence in ClinVar (https://www.ncbi.nlm.nih.gov/clinvar/), conservation (Genomic Evolutionary Rate Profiling—GERP, http://mendel. stanford.edu/SidowLab/downloads/gerp/), and predicted impact on protein structure and function. The pathogenicity of candidate variants was predicted using Combined Annotation Dependent Depletion (CADD, GRCh37-v1.6 version, https://cadd.gs.washington.edu), Sorting Intolerant From Tolerant (SIFT, https://sift.bii.a-star.edu.sg), and Polyphen-2 (http://genetics.bwh.harvard.edu/pph2/). Whole genome sequencing (WGS) was performed, where indicated, on genomic DNA extracted from peripheral blood leukocytes with trio filtration of variants in an exome panel containing 18678 genes. Genetic variants were filtered according to allele frequency ≤ 0.005 in gnomAD for genes associated with autosomal dominant disorders, and ≤ 0.01 for remaining variants. American College of Medical Genetics and Genomics and the Association for Molecular Pathology (ACMG/AMP) guidelines were used to classify candidate variants[34]. Sanger sequencing was performed to validate the detected variants and for segregation analysis. *ABCC9* variants are reported according to RefSeq NM_005691 (GenBank NC_000012.12), using HGVS recommendations[35]. The variants were submitted to the Leiden Open Variation Database (LOVD,

https://www.lovd.nl) with the following accession numbers: #00428407, #00428408, #00428409, #00428410, #00435232, #00435233, and #00435234.

Minigene splicing assay

RNA studies assaying effects of the c.284+1G>A and c.4212-1G>T canonical splice variants were performed as previously described[36,37]. Coding exons 2 (142 bp) and 35 (104 bp), with flanking intronic sequences were directly PCR amplified from a control individual and each proband with primers containing additional restriction sites (for exons 2 and 35, respectively: forward primers with a *Xho*I restriction site: 5'-aattctcgagCCATGTTGTCATCCAGAGTTG-3' and 5'-aattctcgagTGGCAGCACAGCTGATCTAA-3' and reverse primers with a *Bam*HI restriction site: 5'-attggatccCAACAAACCTCCGTGACTCAA-3' and 5'-attggatccCAATGACCTGTACCCACCAA-3'). PCR fragments were ligated into the pSPL3 exon trapping vector between exon A and exon B and confirmed by Sanger sequencing.

Vectors containing the *ABCC9* c.284+1G>A or c.4212-1G>T variants or wild-type sequences were transfected into HEK 293T cells (ATCC). An empty vector and transfection negative reactions were included as controls. Transfected cells were harvested 24 hours after transfection. Total RNA was extracted using miRNeasy Mini Kit (Qiagen) and reverse transcribed using a High-Capacity RNA-to-cDNA Kit (Applied Biosystems). cDNA was PCR amplified using forward (5'-TCTGAGTCACCTGGACAACC-3') and reverse (5'-ATCTCAGTGGTATTTGTGAGC-3') primers. Amplified fragments were visualized by gel electrophoresis and Sanger sequenced.

Recombinant K_{ATP} channel studies

Human SUR2A (accession no. NM_005691) encoding sequences were synthesized and cloned into pcDNA3.1(-) using *Nhe*I and *Xho*I endonucleases. HEK293 cells (Millipore Sigma) were transfected (Fugene 6, Promega) with wild-type pcDNA3.1_mKir6.2 (GenBankTM accession no. D50581.1) and wild-type or mutant hSUR2A constructs in addition to pcDNA3.1_eGFP for

visual detection of transfection. Cells transfected with pcDNA3.1-eGFP alone were used as a negative control.

Patch clamp recordings were made from cells 36 – 48h post-transfection using an Multiclamp 700B amplifier and Digidata 1550B digitizer (Molecular Devices). Currents recorded in response to voltage ramps from -100 to + 60 mV from a holding potential of -80 mV were sampled at 10 kHz, low-pass filtered at 1 kHz. The bath solution contained (in mM): 136 NaCl, 6 KCl, 2 $CaCl_2$, 1 $MgCl_2$, 10 HEPES, 10 Glucose (pH 7.4 with NaOH). The pipette solution without adenosine triphosphate (ATP) contained (in mM): 140 KCl, 10 NaCl, 1 $MgCl_2$, 10 HEPES, 0.5 $CaCl_2$, 4 K_2PHO_4, and 5 EGTA (pH 7.3 with KOH). To test pinacidil activation, 300 µM ATP (potassium salt) was added to the pipette solution and pinacidil (100 µM) and glibenclamide (10 µM) were administered during recordings. Glass micropipettes were pulled from thin-wall borosilicate glass (Sutter) with resistances of 2.5 – 4 MΩ when filled with pipette solution. Recordings were performed at 20 – 22 ºC. Whole-cell currents were measured immediately after membrane rupture and for 10 minutes thereafter. K_{ATP} currents increased over time in wild-type SUR2A expressing cells as intracellular ATP was diluted by the pipette solution (**Fig. 3A**). Leak-subtraction was applied by measuring conductances at -80 mV (the theoretical reversal potential for potassium in these conditions), and currents at 0 mV after 10 minutes are reported. Patch clamp data were analyzed with a Kruskal-Wallis omnibus test followed by Dunn's tests for pairwise comparisons.

Zebrafish model

Zebrafish development and maintenance

Zebrafish (*Danio rerio*) carrying a 13-base frame-shift deletion (XM_005164706.4 c.2947_2959del) in the *abcc9* gene were initially generated by CRISPR/Cas9 mutation of Tübingen longfin one-cell-stage embryos, as previously described[1,38]. This deletion results in reduced expression of *abcc9* transcripts[1], is predicted to result in truncation of any translated protein (XP_005164763.1 p.Gly983TrpfsTer4), and has been shown to result in a loss of SUR2-dependent K_{ATP} channel expression[39]. Zebrafish were maintained as homozygous SUR2-STOP

mutants, which were crossed to generate larvae used in locomotor assays. SUR2-STOP larvae were compared with larvae from in-crossed Tübingen longfin wild type controls.

Larval locomotor assay

We monitored the swimming behavior of 7 days-post-fertilization (dpf) larvae separated into single wells of a 96-well plate containing 200 µL of E3 media and habituated in the Daniovision (Noldus Wageningen, The Netherlands) recording chamber for 1 h before the start of the experiment. Swimming was monitored over a baseline 1-hour dark period in the absence of followed by a 1-hour dark period after 3 mM pentylenotetrazol (PTZ, Sigma-Millipore) administration. Ethovision XT12 (Noldus) was used to analyze distances swam.

Morphological analysis

Morphological analysis was performed on 7 dpf animals. Larvae were immobilized in a 3% methylcellulose cavity, and images were taken using a stereomicroscope (Leica S6E). Body length, head and eye sizes were measured from scale-calibrated images using ImageJ (National Institutes of Health, Bethesda, Maryland).

Results

Patient descriptions

Nine novel AIMS subjects with homozygous *ABCC9* variants were identified in 7 unrelated families exhibiting clinical features that overlap with those previously observed[1] (**Tables 1, 2**).

Family 1

Patient 1-1 (**Fig. 1**) is the only daughter born to nonconsanguineous healthy parents of Norwegian ancestry. She was delivered in pregnancy week 38 by caesarian section due to

bleeding after an otherwise normal pregnancy. Except for being small for gestational age, the neonatal course was uneventful.

The patient had hypotonia and delayed psychomotor development (**Table 1**). At the age of 6 weeks, she suffered generalized tonic-clonic seizures (GTCS) (**Supplementary Table 1**), but until now has never had seizures again. Neuropsychological examination revealed hypotonia, left sided hemiplegia, spasticity, and anxious behavior. She was overweight and showed lumbar lordosis, bilateral Achilles tendon contractures, and dysmorphic facial features (hypotelorism, broad nasal tip, large upper incisors). Physical examination revealed a small head and short stature.

At the age of 1 she experienced a first episode of coma followed by several similar unexplained episodes during childhood. At the age of 2, an episode of coma/somnolence lasting one week was followed by transient left-sided hemiparesis. During that episode, CK was 1030 U/L initially, but increased to 36000 U/L, leading to diagnosis of rhabdomyolysis. She experienced further similar episodes, some with coma and a slight rise in CK, and some with substantial rhabdomyolysis. A muscle biopsy performed after these episodes showed pathological mitochondria and ragged red muscle fibers, but a later biopsy was deemed normal. No further episodes have occurred in the last 5-6 years. She developed left-sided spastic cerebral palsy after the comatose episodes. The patient complained of easy fatigability with cramping within short walking distances. Gene sequencing panels for neuromuscular disease and known causes of rhabdomyolysis have been negative. Her father has experienced one unexplained episode of compartment syndrome and rhabdomyolysis (**Supplementary Table 2**).

At the age of 1.5 years and 15 years, brain MRI showed mild reduction of white matter volume with squared lateral ventricles, multiple confluent fronto-temporo-parietal signal alterations and periventricular cavitations in the frontal regions resembling severe periventricular leukomalacia (**Fig. 1**). Also observed were thinning of the anterior portion of the corpus callosum and multiple dilated perivascular spaces at the level of the basal ganglia (**Fig. 1**), and slightly smaller volume of the hippocampi (**Supplementary Fig. 1**). Brain MRI spectroscopy performed at the level of the affected white matter and right basal ganglia showed normal spectra. Neuropsychological evaluation in adulthood showed severe intellectual disability. She also has anxiety, and episodes of psychosis, for which she is currently medicated. She lives in a

sheltered home, now aged 31. Cardiac ultrasound was normal at ages 16 and 31 and a recent twenty-four-hour ECG recording displayed no arrythmia.

Trio whole genome sequencing identified the previously reported[1] variant in *ABCC9*(NM_005691): c.1320+1G>A, p.(Ala389_Gln440del). The variant was homozygous in the affected proband, and heterozygous in both parents. No additional disease-causing variants were identified.

Family 2

Patients 2-1 and 2-2 (**Fig.** 1) are affected siblings born to consanguineous healthy parents of Pakistani ancestry. Pregnancy and neonatal course were uneventful, but patient 2-1 was born prematurely and delivered via caesarian section. Both patients were diagnosed with a global impairment of psychomotor development in the first year of life with delayed milestones, delayed speech development and no response to stimuli (**Table 1 and Supplementary Table 1**). Patient 2-1 suffered GTCS at the age of 15 months. EEG revealed multifocal interictal epileptic discharges, predominant over right hemisphere. She has been administered valproic acid and levetiracetam. Neurological examination of both siblings revealed microcephaly, severe cognitive dysfunction, decerebrate posture, spasticity, brisk reflexes, and drooling. Patient 2-1 receives gastrostomy feeding. Auditory brainstem response and audiometry studies were normal. Ophthalmologic evaluation showed bilateral optic disc pallor. Brain MRI at the age of 3 years old showed partial agenesis of the corpus callosum in both children, which was associated with bilateral polymicrogyria and enlarged CSF spaces in Patient 2-2.

Exome sequencing revealed a homozygous (NM_005691): c.2812C>T, p.(Arg938Ter) variant in the affected siblings. Both parents were heterozygous carriers.

Family 3

Patient 3-1 is the affected daughter of consanguineous healthy parents of Egyptian ancestry. Pregnancy and neonatal course were uneventful. Physical examination during infancy revealed psychomotor delay and hypotonia (**Table 1 and Supplementary Table 1**). At the age of 4,

neurological examination revealed microcephaly, spasticity, nystagmus, and anxious behavior. Mild hip girdle weakness and contractures were present, requiring tenotomy. Brain CT performed at 6 months of age showed multiple small calcifications in the periventricular frontal white matter and right basal ganglia. Brain MRI at the age of 9 months showed mild volume reduction of the periventricular white matter with squared appearance of the lateral ventricles, multiple confluent periventricular white matter signal alterations in the fronto-temporo-parietal regions and a thin anterior corpus callosum resembling periventricular leukomalacia (**Fig. 1**).

Exome sequencing revealed the homozygous (NM_005691): c.4212-1G>T variant in the affected proband, both parents were heterozygous carriers.

Family 4

Patient 4-1 is the affected daughter of nonconsanguineous healthy parents of Dutch ancestry. After an uncomplicated pregnancy the neonatal course was complicated by hypotonia and unilateral hip dysplasia at birth, for which tendon release was performed at the age of 18 months, lower extremity asymmetry, scoliosis and lordosis. Feeding problems were reported but growth parameters were within normal range. At 11 years of age, she was diagnosed with psychomotor delay (**Supplementary Table 1**). Neurological examination identified mild cognitive impairment. Brain MRI at the age of 13 years revealed no abnormalities.

Exome sequencing revealed a homozygous (NM_005691): c.1858C>T, p.(Arg620Ter) variant in the affected proband, carried by both heterozygous parents. The family also suffered two intra-uterine fetal deaths (at 31 weeks and 38 weeks of gestation). Both fetuses were homozygous for the c.1858C>T, p.(Arg620Ter) variant. Two healthy brothers did not carry the variant.

Family 5

Patient 5-1 is the daughter of consanguineous healthy parents of Egyptian ancestry, born by cesarian section following an uncomplicated pregnancy. She exhibits defective balance, fatigability, and hypotonia, spasticity, weakness, and hyperreflexia of the lower limbs. Brain

MRI at 10 months of age showed moderate periventricular white matter volume reduction with squared appearance of the lateral ventricles and multiple confluent periventricular white matter signal alterations in the fronto-temporo-parietal regions, resembling a severe periventricular leukomalacia (**Fig. 1**). A small pons and thin corpus callosum were also noted. Brain CT at 2 years of age showed no calcifications.

Exome sequencing revealed the presence of the (NM_005691): c.1234C>T, p.(Gln412Ter) variant in the homozygous state for the affected proband, carried by both heterozygous parents.

Family 6

Patient 6-1 (**Fig. 1**) is the second child of healthy, unrelated Norwegian parents. He was born prematurely at 33 + 6 weeks of gestation. Apgar score was 5-8-9 (at 1, 5, and 10 minutes), and he was resuscitated. Delayed psychomotor development became evident, and he was diagnosed with unilateral cerebral palsy. Brain MRI at 7 years of age displayed mild reduction of periventricular white matter in the occipito-parietal regions with squared appearance of the lateral ventricles. There were multiple confluent fronto-parietal signal alterations, mainly in the periventricular regions, resembling periventricular leukomalacia. Brain CT performed at the same age showed multiple small calcifications in the deep fronto-parietal white matter, and faint linear cortical calcifications in the perirolandic regions (**Fig. 1**) as well as bilateral calcifications in grey matter. Achilles tendon contracture was treated with botulinum toxin and Achilles tendon lengthening was performed at seven years of age. He is easily tired when exercising. He is microcephalic, with growth otherwise in the normal range. He was diagnosed with mild intellectual disability by formal neuropsychological testing, has anxiety and takes medication for attention deficit disorder (**Supplementary Table 1**). At the age of 13, he experienced GTCS, with electric activity suspicious for epilepsy in a sleep-deprived EEG.

Patient 6-2 is the third child in the family and the sister of patient 6-1. Her mother had premature rupture of the membranes in gestational week 32. She was born at 37 weeks, with an uneventful neonatal course. Global developmental delay was evident. A diagnosis of bilateral spastic cerebral palsy was given at age 1.5 years, and brain MRI showed very mild white matter

volume reduction and fronto-parietal white matter signal changes resembling periventricular leukomalacia. Achilles tendon contractures were treated with botulinum toxin injections, and at six years of age gastrocnemius release and tendon lengthening were performed. Motor fatigability is evident. At nine years of age she had a formal neurocognitive test and was diagnosed with learning difficulties - with skills in the lower normal range. Genome sequencing of both affected siblings revealed homozygosity for the (NM_005691): c.284+1G>A variant with the parents being heterozygous carriers.

Family 7

Patient 7-1 is a 36-year-old female and one of five children of healthy British Pakistani parents, who are first cousins. She was born at term after an unremarkable pregnancy. She was described as a "floppy baby" and had feeding difficulties. She underwent a patent ductus arteriosus closure procedure around 6 months of age. There were several admissions to hospital with diarrheal illnesses in early life. She was diagnosed with acquired hypothyroidism around age 13 years. Development was globally delayed, and she attended a special school for children with additional educational needs from age 5 years (**Table 1 and Supplementary Table 1**). She has a mild intellectual disability and lives with her mother, requiring prompting with personal care and some supervision or assistance with most activities of daily living. Aside from relative microcephaly, there was no overt craniofacial dysmorphism. She has a slender, long-limbed habitus, with relatively long fingers. Skin of her hands was affected by dermatitis. There is no history of epilepsy, and she has never had brain imaging.

Several episodes of acute psychosis characterized by pressured speech and paranoia have been reported. She has received a diagnosis of autism, associated with symptoms of anxiety and mood lability. There is no formal diagnosis of a muscle disorder, but family reports that she complains of fatigue even after just a short walk. Reflexes were normal. She would not comply with formal muscle examination but was able to walk on tiptoes and heels.

Trio-based analysis of the DDG2P gene panel (https://www.ebi.ac.uk/gene2phenotype) from whole exome sequence data revealed the presence of the (NM_005691): c.3747del,

p.(Leu1250TrpfsTer9) variant in the homozygous state for the affected proband, carried by both heterozygous parents.

Family 8

In addition to the above cases, we also identified a further family from Saudi Arabia in which both parents carried the *ABCC9* c.2140_2141del, p.(Leu714SerfsTer7) variant and who experienced two intrauterine fetal deaths (IUFDs) at 8 months of pregnancy of unknown etiology. A further daughter died 20 days after birth following apnea. Molecular autopsy by proxy[40,41] was conducted using exome sequencing on parental DNA who were found to share the carrier status for the (NM_005691): c.2140_2141del, p.(Leu714SerfsTer7) variant.

ABCC9 variants

Exome and genome sequencing identified eight LoF, or predicted LoF, variants in *ABCC9* (**Table 1, Fig. 2**). All affected individuals were homozygous for *ABCC9* variants and Sanger sequencing confirmed that unaffected parents were carriers. The variants are rare in the general population (max allele frequency 0.000088) and absent in homozygous state in the gnomAD database. They are predicted to result either in nonsense-mediated mRNA decay (NMD) or in the formation of a truncated protein, leading to complete loss of *ABCC9* protein function. All the reported *ABCC9* variants are classified as pathogenic or likely pathogenic according to the ACMG criteria.

The intronic c.4212-1G>T variant identified in family 3 was assessed in mini-gene splicing studies. Wild-type and mutant *ABCC9* coding exon 35 (notated as exon 37 in Ensembl transcript ENST00000261200.9) and flanking intronic regions were cloned into pSPL3 mini-gene constructs which were transfected into HEK 293T cells. Expression of the WT intron-exon-intron sequence resulted in the expected canonical splicing (**Fig. 2A,B**). In contrast the c.4212-1G>T variant resulted in activation of a cryptic splice acceptor site leading to deletion of 11 nucleotides and a subsequent frameshift (c.4214_4224del, r.4214_4224del, p.(Phe1405SerfsTer8) (**Fig. 2A-C**). The c.284+1G>A variant resulted in exon skipping of coding

exon 2 (142 bp) in the mini-gene assay, which in the native sequence would result in a frame-shift and the p.(Phe49GlyfsTer13) truncation.

Heterozygous family members

Clinical details from heterozygous parents and relatives are limited but, as shown in **Supplementary Table 2**, no consistent pathological findings were observed amongst 16 genotyped relatives. Rhabdomyolysis was reported for the carrier father of 1-1, epileptic encephalopathy in the heterozygous maternal aunt of individual 1-1, and dilated cardiomyopathy was diagnosed at age 60 in the father of family 2 in the original report of AIMS[1]. Normal cardiac function was confirmed in 3 further heterozygous relatives aged > 50 years old.

Effects on K_{ATP} channel function

The novel variants reported here result, or for the 284+1G>A and c.4212-1G>T variants, are predicted to result, in premature stop codons in *ABCC9* transcripts which are expected to undergo nonsense-mediated decay *in vivo*. To determine whether any truncated protein, from transcripts which might escape nonsense-mediated decay, would be functional, we co-expressed WT or mutant SUR2A with Kir6.2 in HEK293 cells (**Fig. 3A**). Robust potassium conductances were observed in cells expressing WT SUR2A in whole-cell recordings after dilution of intracellular nucleotides with a nucleotide-free pipette solution (**Fig. 3B**). No K_{ATP} channel activity was observed in cells transfected with SUR2[Arg620Ter], SUR2[Arg938Ter], SUR2[Phe1405SerfsTer8], or SUR2[Leu714SerfsTer7], and whole cell currents were essentially identical to cells transfected with GFP alone (**Fig. 3B,C**). Therefore, as also previously shown for the c.1320+1G>A, p.Ala389_Gln440del variant[1], all tested *ABCC9* variants result in a complete loss of recombinant K_{ATP} channel functional expression.

K_{ATP} channel openers (KCOs) are used clinically for hypertension and angina pectoris[42]. These drugs bind at a common site in SUR2, formed of multiple transmembrane helices from TMD1 and TMD2[43,44]. All truncations identified here are expected to abolish or disrupt this binding site, with the possible exception of SUR2[Phe1405SerfsTer8] in which the truncation

occurs after TMD2. To test if KCO sensitivity was retained in SUR2[Phe1405SerfsTer8] mutant channels, we performed whole-cell patch clamp recordings with 300 μM ATP in the patch pipette before applying pinacidil to activate channels, followed by application of the K_{ATP} inhibitor glibenclamide. WT channels exhibited robust pinacidil and glibenclamide sensitivity as expected, but no channel activity was observed in cells transfected with Kir6.2 and SUR2[Phe1405SerfsTer8], even in the presence of pinacidil (**Fig. 3D,E**). Therefore, KCOs are highly unlikely to be effective for all AIMS mutations identified to date.

Seizure susceptibility in SUR2 loss-of-function zebrafish

Seizures were reported in 4 novel AIMS subjects. Locomotor activity in SUR2-STOP and WT zebrafish larvae (7 dpf) was assessed by automated swimming tracking. As previously reported[1], SUR2-STOP larvae exhibit reduced basal locomotion, compared to WT controls, potentially due to skeletal myopathy (**Fig. 4A**). Administration of the pro-convulsive GABA receptor antagonist, pentylenetetrazole (PTZ; 3mM), to WT larvae provoked a small but significant increase in locomotion, reflecting a mild drug-induced hyperactivity. Contrastingly, locomotion in SUR2-STOP larvae was dramatically increased by PTZ, such that the relative activity of mutant larvae in PTZ, normalized to basal activity, increased to a much greater extent than observed in WT larvae (**Fig. 4A-C**). This suggests abnormal neural excitatory/inhibitory balance in SUR2-STOP larvae, consistent with a neurodevelopmental phenotype and increased seizure susceptibility.

SUR2-STOP larvae also exhibited significantly smaller body length compared to WT controls (**Fig. 4D**), consistent with the small stature observed in the clinical subjects described. SUR2-STOP larvae exhibited facial dysmorphology, with decreased inter-eye distance and eye size, but gross head dimensions were not significantly different (**Fig.4E-H)**.

Discussion

We identified seven homozygous *ABCC9* LoF variants in nine affected individuals from seven unrelated families of different ancestry. Seven variants are novel while the c.1320+1G>A (p.Ala389_Gln440) variant of Patient 1-1 is the same detected in the two previously reported

Norwegian families. Notably, Family 1 is also from Norway, and this variant is enriched in neighboring northern Finland by two orders of magnitude relative to non-Finnish European populations, suggesting a founder effect (Sequencing Initiative Suomi project (SISu), Institute for Molecular Medicine Finland (FIMM), University of Helsinki, Finland (URL: http://sisuproject.fi) [SISu v4.1, April, 2023] 12:22063090; rs139620148). The p.Ala389_Gln440 deletion arises from the in-frame deletion of exon 8 and results in a complete loss of plasmalemmal K_{ATP} function upon heterologous expression[1]. The novel variants in *ABCC9* result, or are predicted to result, in premature stop codons, and are expected to lead to nonsense-mediated decay and/or major truncation of the SUR2 protein, with deleterious effects on SUR2-dependent K_{ATP} channels. Characterization of recombinant channels demonstrates that p.Arg620Ter, p.Arg938Ter, p.Phe1405SerfsTer8, and p.Leu714SerfsTer7 all result in complete loss of K_{ATP} function. The c.1234C>T, p.(Gln412Ter); c.284+1G>A, p.(Phe49GlyfsTer13); and c.3747del, p.(Leu1250TrpfsTer9) variants were most recently identified, and are expected to result in complete LoF.

Comparison of new patients with initial patients

Previously reported patients belonged to two families in which the same variant (c.1320+1G>A) segregated in six affected members[1]. These subjects presented with an overlapping spectrum of clinical features, with a core neurological phenotype consisting of psychomotor delay, intellectual disability, anxious behavior, hyperreflexia, and hypotonia in childhood (**Table 2**). Additionally, they exhibited fatigability and myopathic features. The new cohort showed conserved features, including nystagmus, seizures, tendon abnormalities, and lumbar lordosis, but also present with additional distinctive pathologies, expanding the *ABCC9*-related phenotype spectrum (**Table 2 and Supplementary Table 1**). Neurological examination revealed spasticity and exaggerated deep tendon reflexes in six out of nine subjects, with two subjects showing severe decerebrate postures. Progressive microcephaly diagnoses were made for six out of nine subjects. A peculiar clinical course was observed in Patient 1-1, who harbored the same variant detected in the first two Norwegian families. This subject exhibited multiple episodes of loss-of-consciousness, which occurred in combination with rhabdomyolysis. One patient in the original cohort experienced an episode of coma, as well as transient white matter changes on MRI,

without significant elevation of creatine kinase. Intriguingly, two older female patients experienced episodes of psychosis of unknown mechanisms.

While systolic dysfunction was described in two previous cases[1], no significant cardiac disorder was identified in our study. Interestingly, the subjects with cardiac dysfunction were 29 years or older at initial diagnosis, suggesting that a follow-up is important in *ABCC9* patients, as cardiac dysfunction may emerge later in the disease course.

Comparison of brain MRI findings

Brain abnormalities observed in previous *ABCC9* subjects consisted of white matter signal alterations localized in the centrum semiovale or in the periventricular regions associated with brain calcifications in one case.[34] Similar findings were observed in Patients 1-1, 3-1, 5-1, 6-1 and 6-2 from our cohort. Of note, we also found brain calcifications in two patients; in the frontal periventricular white matter and right basal ganglia in one subject (Patient 3-1) and in both the white and grey matter in another subject (Patient 6-1). In addition, white matter cavitations were detected in the frontal regions in Patient 1-1.

White matter changes in these patients frequently resemble periventricular leukomalacia (PVL). PVL is often the end-stage of white matter damage in preterm infants, with a likely underlying inflammatory mechanism, however, recent evidence demonstrates that PVL-like features may present in some genetic conditions in the absence of perinatal risk factors. This neuroradiological pattern has been associated with *COL4A1/A2*, *AMPD2*, *TBCK*, and *NSD1* variants, as well as dehydrogenase deficiency and incontinentia pigmentii[45-53]. PVL has also been found in subjects with *WWOX*, *SPATA5L1*, *WIPI2* and *EZH2* variants[54-56]. Therefore, rather than a specific entity, PVL might represent a radiological sign of white matter involvement with specific prenatal timing and mechanisms, that in certain clinical scenarios may help with diagnosis of a genetic condition. Notably, in subjects with developmental delay, intellectual disability, and fatigability (**Table 2**) the presence of PVL-like changes associated with progressive microcephaly, temporal white matter involvement, and scattered calcifications, should raise the suspicion of an *ABCC9*-related disorder.

We detected additional novel brain abnormalities in some subjects in line with a white matter involvement; hypoplasia or partial agenesis of the corpus callosum was identified in five patients (Patients 1-1, 2-1, 2-2, 3-1 and 5-1). Thinning of the corpus callosum was mainly related to the white matter volume reduction and callosal agenesis is likely related to a primary white matter developmental disorder. Bilateral polymicrogyria was detected in Patient 2-2. These neuroradiological manifestations expand the spectrum of brain MRI abnormalities in *ABCC9* patients, suggesting that white matter is primarily involved in these individuals with a PVL-like pattern, but cerebral malformations may occasionally be part of the spectrum.

AIMS pathology in a zebrafish model

Consistent dysmorphic features were observed in the original AIMS patients, including hypotelorism, broad nasal tip, flat face and thin upper lip vermillion[1]. In the current study, facial features were described as normal for five subjects, with the Norwegian individual (1-1) again exhibiting hypotelorism and broad nasal tip, and one further subject (5-1) exhibiting other dysmorphology (**Table 2 and Supplementary Table 1).** LoF SUR2 (SUR2-STOP) zebrafish larvae display reduced intra-orbital distances and eye diameters, linking SUR2 dysfunction with abnormal facial development.

Epilepsy with unconscious episodes was reported in one original AIMS patient[1]. Here, patient 1-1 had one unexplained generalized seizures\ episode in the neonatal period, but none since, and three others (2-1, 4-1 and 6-1) also experienced seizures as children. Therefore, multiple incidences of epileptic activity have now been observed in unrelated *ABCC9* LoF AIMS patients. To determine whether SUR2 LoF increases seizure susceptibility, we subjected WT and SUR2-STOP zebrafish larvae to PTZ-sensitivity tests. SUR2-STOP larvae exhibit reduced basal locomotion, which is likely due to skeletal muscle weakness[1,60], but small size or altered vision due to craniofacial dysmorphology in SUR2-STOP fish might also contribute. The epileptogenic GABA-A receptor antagonist PTZ had a markedly greater effect on locomotion in SUR2-STOP larvae than WT controls, consistent with increased seizure-susceptibility, and providing experimental evidence of pro-epileptic effects of SUR2 LoF.

Intrauterine fetal death in *ABCC9* variant families

Family 4 suffered two IUFDs of fetuses homozygous for the c.1858C>T, p.(Arg620Ter) variant. In family 8, who experienced multiple incidences of IUFD, DNA from two fetuses and one neonatal death was unobtainable, but molecular autopsy by proxy showed both parents to be carriers of the c.2140_2141del, p.(Leu714SerfsTer7) variant. In the first report of AIMS[1], one family elected to terminate a pregnancy in week 20 due to severe skeletal dysplasia in the fetus. However, sequencing revealed the affected fetus to be only heterozygous for the c.1320+1G>A variant. Whether IUFD might represent the severe end of the AIMS spectrum is left to determine.

Pathophysiology and variable severity in AIMS

How *ABCC9* mutations and loss of SUR2-dependent K_{ATP} channel activity result in these diverse neurological and developmental pathologies is not yet fully understood. Neuronal K_{ATP} channels, involved in nutrient and metabolic sensing, have been shown to play neuroprotective roles in ischemia, and protect against hypoxia- and drug-induced epilepsy, where channel activation reduces excitability[61-64]. SUR1 is reportedly the predominant subunit in most neuronal populations[65,66], although SUR2 mRNA has been identified in multiple neurons in rodents, including hippocampal CA1 pyramidal and dentate gyrus granule cells, and dopaminergic excitatory neurons of the substantia nigra pars compacta. K_{ATP} channels in these neurons show an intermediate pharmacological profile that is suggestive of mixed SUR1/SUR2/Kir6.2 channel composition[27-29]. Single-cell mRNA expression databases reveal *ABCC9* expression in excitatory neurons and glial cells[67] (https://www.proteinatlas.org/ENSG00000069431-ABCC9/single+cell+type). Of note, *ABCC9* polymorphisms have also been associated with hippocampal sclerosis in aging, though a mechanism is again not yet known[26,68]. There were no signs of hippocampal sclerosis were in the patients studied here, although, subject 1-1 demonstrated slightly smaller hippocampi without associated T2/FLAIR signal alterations and subject 3-1 had bilateral incomplete hippocampal rotation (**Supplementary Fig. 1**).

A key role for SUR2-dependent K_{ATP} channels in the cerebral vasculature is also emerging, with smooth muscle or pericyte K_{ATP} activation associated with neurovascular

coupling[69]. Cerebrovascular abnormalities are also seen in Cantú Syndrome, including white matter hyperintensities that potentially arise from abnormal cerebral blood flow. Therefore, both overactivity and loss of K_{ATP} channels in the cerebral vasculature might converge in limiting dynamic nutrient and oxygen supply. 24 % of Cantú Syndrome subjects self-reported history of seizures in a recent study[57], but the pathophysiological basis is yet to be determined. Additionally, severe GoF mutations in *KCNJ11* (Kir6.2) and *ABCC8* (SUR1) are associated with developmental delay, epilepsy and neonatal diabetes (DEND)[70-73]. Neurodevelopmental abnormalities in AIMS may arise from neuronal and/or non-neuronal mechanisms, such as altered vascular or astrocyte dysfunction. Future studies of tissue specific *ABCC9* perturbation in animal models may provide insights.

The patients we report here exhibit a spectrum of neurodevelopmental pathology ranging from near normal cognition (Patient 3-1) to severe intellectual disability and decerebrate posture. Recombinant analysis of truncated SUR2 subunits reveal that they are completely non-functional. Interestingly, intellectual disability was mild in five out of six of the previously reported subjects with the c.1320+1G>A splice site mutation. Intellectual disability was moderate in one, and severe in the individual with the same genotype in this cohort. The mildly affected Patient 3-1 here, and Patients 6-1 and 6-2 with mild intellectual disability and only learning difficulties, respectively, also exhibit splice-site mutations. It is tempting to speculate that some transcripts might escape aberrant splicing *in vivo*, and thereby moderate severity, although it is also possible that some patients escape early traumatic consequences or otherwise avoid a developmental threshold effect leading to severe disability.

Fatigability, weakness, and cramping were consistently observed in the original AIMS subjects and in these new individuals. SUR2 subunits are critically required for K_{ATP} function in muscle, therefore it is likely that muscle pathology in AIMS arises in a skeletal muscle delimited mechanism[60]. Studies of Kir6.2 and SUR2 knockout mice show that the activation of K_{ATP} channels protects myofibers from sustained depolarization and cytosolic calcium overload[23,24,31], and both fatigability and involuntary muscle contraction results from K_{ATP} LoF in skeletal muscle specifically[60]. It is possible that the episodes of rhabdomyolysis reported here for Patient 1-1, may occur due to muscle breakdown in the absence of the myoprotective effects of K_{ATP} channels. Her otherwise unaffected carrier father also experienced an episode of rhabdomyolysis.

No obvious reason has been found by gene sequencing with a neuromuscular panel in the father, or in the whole exome sequencing of patient 1-1, but it remains possible that other genetic factors may contribute.

Conclusions

Our studies further confirm the association of LoF variants in *ABCC9* with a neurodevelopmental disorder featuring cognitive impairment, childhood hypotonia, seizures, contractures, spasticity, and myopathic features, alongside white matter abnormalities often resembling periventricular leukomalacia. Identification of additional genetically confirmed individuals helps to define the phenotypic spectrum and pathological mechanisms of AIMS, and reveals that some patients are severely affected by neurological involvements and brain abnormalities. *In vivo* studies of *abcc9* LoF in zebrafish show an exacerbated motor response to pentylenetetrazole, consistent with increased seizure susceptibility.

Data availability

All data in this study are available within the article and Supplementary material.

Acknowledgements

We wish to thank Yngve Sejersted, geneticist at the Department of Medical Genetics, Oslo University Hospital for analysis and discussion and to Mais Hashem at the King Faisal Specialist Hospital and Research Centre, Riaydh, Saudi Arabia for her help as a clinical research coordinator. BV is a member of the European Reference Network on Rare Congenital Malformations and Rare Intellectual Disability (ERN-ITHACA) [EU Framework Partnership Agreement ID: 3HP-HP-FPA ERN-01-2016/739516].

Funding

This research was funded in part, by the Wellcome Trust (WT093205MA, WT104033AIA). SE was supported by an MRC strategic award to establish an International Centre for Genomic Medicine in Neuromuscular Diseases (ICGNMD) MR/S005021/1. We are grateful for the essential support from patients and families and funding to the UCL team from The Wellcome Trust, The MRC, The MSA Trust, The National Institute for Health Research University College London Hospitals Biomedical Research Centre, The Michael J Fox Foundation (MJFF), BBSRC, The Fidelity Trust, Rosetrees Trust, Ataxia UK, Brain Research UK, Sparks GOSH Charity, Alzheimer's Research UK (ARUK) and CureDRPLA. BV is funded by the Deutsche Forschungsgemeinschaft (DFG, German Research Foundation) VO 2138/7-1 grant 469177153. CGN is supported by NIH Award R35 HL140024. CMc is supported by NIH Award K99/R00 HL150277.

Competing interests

The authors declare no competing interests.

Supplementary material

Supplementary material is available at *Brain* online.

References

1 Smeland, M. F. *et al.* ABCC9-related Intellectual disability Myopathy Syndrome is a KATP channelopathy with loss-of-function mutations in ABCC9. *Nature Communications* **10**, 4457 (2019). https://doi.org:10.1038/s41467-019-12428-7

2 Nichols, C. G. KATP channels as molecular sensors of cellular metabolism. *Nature* **440**, 470-476 (2006). https://doi.org:10.1038/nature04711

3 Zerangue, N., Schwappach, B., Jan, Y. N. & Jan, L. Y. A new ER trafficking signal regulates the subunit stoichiometry of plasma membrane K(ATP) channels. *Neuron* **22**, 537-548 (1999). https://doi.org:10.1016/s0896-6273(00)80708-4

4 Schwappach, B., Zerangue, N., Jan, Y. N. & Jan, L. Y. Molecular basis for K(ATP) assembly: transmembrane interactions mediate association of a K+ channel with an ABC transporter. *Neuron* **26**, 155-167 (2000). https://doi.org:10.1016/s0896-6273(00)81146-0

5 Inagaki, N. *et al.* Reconstitution of IKATP: an inward rectifier subunit plus the sulfonylurea receptor. *Science* **270**, 1166-1170 (1995). https://doi.org:10.1126/science.270.5239.1166

6 Inagaki, N. *et al.* A Family of Sulfonylurea Receptors Determines the Pharmacological Properties of ATP-Sensitive K+ Channels. *Neuron* **16**, 1011-1017 (1996). https://doi.org:10.1016/s0896-6273(00)80124-5

7 Clement, J. P. *et al.* Association and Stoichiometry of KATP Channel Subunits. *Neuron* **18**, 827-838 (1997). https://doi.org:10.1016/s0896-6273(00)80321-9

8 Shyng, S. L. & Nichols, C. G. Octameric Stoichiometry of the KATPChannel Complex. *The Journal of General Physiology* **110**, 655-664 (1997). https://doi.org:10.1085/jgp.110.6.655

9 Tucker, S. J., Gribble, F. M., Zhao, C., Trapp, S. & Ashcroft, F. M. Truncation of Kir6.2 produces ATP-sensitive K+ channels in the absence of the sulphonylurea receptor. *Nature* **387**, 179-183 (1997). https://doi.org:10.1038/387179a0

10 Sharma, N. *et al.* The C terminus of SUR1 is required for trafficking of KATP channels. *J Biol Chem* **274**, 20628-20632 (1999). https://doi.org:10.1074/jbc.274.29.20628

11 Bienengraeber, M. *et al.* ABCC9 mutations identified in human dilated cardiomyopathy disrupt catalytic KATP channel gating. *Nat Genet* **36**, 382-387 (2004). https://doi.org:10.1038/ng1329

12 Aguilar-Bryan, L. & Bryan, J. Molecular biology of adenosine triphosphate-sensitive potassium channels. *Endocr Rev* **20**, 101-135 (1999). https://doi.org:10.1210/edrv.20.2.0361

13 Foster, M. N. & Coetzee, W. A. KATP Channels in the Cardiovascular System. *Physiol Rev* **96**, 177-252 (2016). https://doi.org:10.1152/physrev.00003.2015

14 Flagg, T. P., Enkvetchakul, D., Koster, J. C. & Nichols, C. G. Muscle KATP channels: recent insights to energy sensing and myoprotection. *Physiol Rev* **90**, 799-829 (2010). https://doi.org:10.1152/physrev.00027.2009

15 Chutkow, W. A. *et al.* Episodic coronary artery vasospasm and hypertension develop in the absence of Sur2 KATP channels. *Journal of Clinical Investigation* **110**, 203-208 (2002). https://doi.org:10.1172/jci0215672

16 Miki, T. *et al.* Mouse model of Prinzmetal angina by disruption of the inward rectifier Kir6.1. *Nat Med* **8**, 466-472 (2002). https://doi.org:10.1038/nm0502-466

17 Li, A. *et al.* Hypotension due to Kir6.1 gain-of-function in vascular smooth muscle. *J Am Heart Assoc* **2**, e000365 (2013). https://doi.org:10.1161/JAHA.113.000365

18 York, N. W. *et al.* Kir6.1- and SUR2-dependent KATP over-activity disrupts intestinal motility in murine models of Cantu Syndrome. *JCI Insight* (2020). https://doi.org:10.1172/jci.insight.141443

19 Davis, M. J. *et al.* Kir6.1-dependent K(ATP) channels in lymphatic smooth muscle and vessel dysfunction in mice with Kir6.1 gain-of-function. *J Physiol* **598**, 3107-3127 (2020). https://doi.org:10.1113/JP279612

20 Zingman, L. V. *et al.* Kir6.2 is required for adaptation to stress. *Proc Natl Acad Sci U S A* **99**, 13278-13283 (2002). https://doi.org:10.1073/pnas.212315199

21 Zhu, Z. *et al.* Sarcolemmal ATP-sensitive potassium channels modulate skeletal muscle function under low-intensity workloads. *J Gen Physiol* **143**, 119-134 (2014). https://doi.org:10.1085/jgp.201311063

22 Gong, B., Legault, D., Miki, T., Seino, S. & Renaud, J. M. KATP channels depress force by reducing action potential amplitude in mouse EDL and soleus muscle. *Am J Physiol Cell Physiol* **285**, C1464-1474 (2003). https://doi.org:10.1152/ajpcell.00278.2003

23 Cifelli, C., Boudreault, L., Gong, B., Bercier, J. P. & Renaud, J. M. Contractile dysfunctions in ATP-dependent K+ channel-deficient mouse muscle during fatigue

involve excessive depolarization and Ca2+ influx through L-type Ca2+ channels. *Exp Physiol* **93**, 1126-1138 (2008). https://doi.org:10.1113/expphysiol.2008.042572

24 Cifelli, C. *et al.* KATP channel deficiency in mouse flexor digitorum brevis causes fibre damage and impairs Ca2+ release and force development during fatigue in vitro. *J Physiol* **582**, 843-857 (2007). https://doi.org:10.1113/jphysiol.2007.130955

25 McClenaghan, C. & Nichols, C. G. Kir6.1 and SUR2B in Cantu syndrome. *Am J Physiol Cell Physiol* **323**, C920-C935 (2022). https://doi.org:10.1152/ajpcell.00154.2022

26 Nelson, P. T. *et al.* ABCC9/SUR2 in the brain: Implications for hippocampal sclerosis of aging and a potential therapeutic target. *Ageing Res Rev* **24**, 111-125 (2015). https://doi.org:10.1016/j.arr.2015.07.007

27 Liss, B., Bruns, R. & Roeper, J. Alternative sulfonylurea receptor expression defines metabolic sensitivity of K-ATP channels in dopaminergic midbrain neurons. *EMBO J* **18**, 833-846 (1999). https://doi.org:10.1093/emboj/18.4.833

28 Pelletier, M. R., Pahapill, P. A., Pennefather, P. S. & Carlen, P. L. Analysis of single K(ATP) channels in mammalian dentate gyrus granule cells. *J Neurophysiol* **84**, 2291-2301 (2000). https://doi.org:10.1152/jn.2000.84.5.2291

29 Zawar, C., Plant, T. D., Schirra, C., Konnerth, A. & Neumcke, B. Cell-type specific expression of ATP-sensitive potassium channels in the rat hippocampus. *J Physiol* **514 (Pt 2)**, 327-341 (1999). https://doi.org:10.1111/j.1469-7793.1999.315ae.x

30 Kane, G. C. *et al.* KCNJ11 gene knockout of the Kir6.2 KATP channel causes maladaptive remodeling and heart failure in hypertension. *Hum Mol Genet* **15**, 2285-2297 (2006). https://doi.org:10.1093/hmg/ddl154

31 Stoller, D. *et al.* Impaired exercise tolerance and skeletal muscle myopathy in sulfonylurea receptor-2 mutant mice. *Am J Physiol Regul Integr Comp Physiol* **297**, R1144-1153 (2009). https://doi.org:10.1152/ajpregu.00081.2009

32 Selvin, D. & Renaud, J. M. Changes in myoplasmic Ca2+ during fatigue differ between FDB fibers, between glibenclamide-exposed and Kir6.2-/- fibers and are further modulated by verapamil. *Physiol Rep* **3** (2015). https://doi.org:10.14814/phy2.12303

33 Efthymiou, S. *et al.* Biallelic mutations in neurofascin cause neurodevelopmental impairment and peripheral demyelination. *Brain* **142**, 2948-2964 (2019). https://doi.org:10.1093/brain/awz248

34 Richards, S. *et al.* Standards and guidelines for the interpretation of sequence variants: a joint consensus recommendation of the American College of Medical Genetics and Genomics and the Association for Molecular Pathology. *Genet Med* **17**, 405-424 (2015). https://doi.org:10.1038/gim.2015.30

35 den Dunnen, J. T. *et al.* HGVS Recommendations for the Description of Sequence Variants: 2016 Update. *Hum Mutat* **37**, 564-569 (2016). https://doi.org:10.1002/humu.22981

36 Tompson, S. W. & Young, T. L. Assaying the Effects of Splice Site Variants by Exon Trapping in a Mammalian Cell Line. *Bio Protoc* **7** (2017). https://doi.org:10.21769/BioProtoc.2281

37 Rad, A. *et al.* Aberrant COL11A1 splicing causes prelingual autosomal dominant nonsyndromic hearing loss in the DFNA37 locus. *Hum Mutat* **42**, 25-30 (2021). https://doi.org:10.1002/humu.24136

38 Tessadori, F. *et al.* Effective CRISPR/Cas9-based nucleotide editing in zebrafish to model human genetic cardiovascular disorders. *Dis Model Mech* **11** (2018). https://doi.org:10.1242/dmm.035469

39 Singareddy, S. S. *et al.* ATP-sensitive potassium channels in zebrafish cardiac and vascular smooth muscle. *J Physiol* **600**, 299-312 (2022). https://doi.org:10.1113/JP282157

40 Monies, D. *et al.* Lessons Learned from Large-Scale, First-Tier Clinical Exome Sequencing in a Highly Consanguineous Population. *Am J Hum Genet* **104**, 1182-1201 (2019). https://doi.org:10.1016/j.ajhg.2019.04.011

41 Shamseldin, H. E. *et al.* Molecular autopsy in maternal-fetal medicine. *Genet Med* **20**, 420-427 (2018). https://doi.org:10.1038/gim.2017.111

42 Jahangir, A. & Terzic, A. K(ATP) channel therapeutics at the bedside. *J Mol Cell Cardiol* **39**, 99-112 (2005). https://doi.org:10.1016/j.yjmcc.2005.04.006

43 Moreau, C., Jacquet, H., Prost, A. L., D'Hahan, N. & Vivaudou, M. The molecular basis of the specificity of action of K(ATP) channel openers. *EMBO J* **19**, 6644-6651 (2000). https://doi.org:10.1093/emboj/19.24.6644

44 Ding, D. *et al.* Structural identification of vasodilator binding sites on the SUR2 subunit. *Nat Commun* **13**, 2675 (2022). https://doi.org:10.1038/s41467-022-30428-y

45 Reddy, N. *et al.* Neuroradiological Mimics of Periventricular Leukomalacia. *J Child Neurol* **37**, 151-167 (2022). https://doi.org:10.1177/08830738211026052

46 Nicita, F. *et al.* Leukoencephalopathy with spot-like calcifications caused by recessive COL4A2 variants. *Clin Neurol Neurosurg* **225**, 107584 (2023). https://doi.org:10.1016/j.clineuro.2022.107584

47 Livingston, J. *et al.* COL4A1 mutations associated with a characteristic pattern of intracranial calcification. *Neuropediatrics* **42**, 227-233 (2011). https://doi.org:10.1055/s-0031-1295493

48 Accogli, A. *et al.* Novel AMPD2 mutation in pontocerebellar hypoplasia, dysmorphisms, and teeth abnormalities. *Neurol Genet* **3**, e179 (2017). https://doi.org:10.1212/NXG.0000000000000179

49 Scola, E. *et al.* Neuroradiological findings in three cases of pontocerebellar hypoplasia type 9 due to AMPD2 mutation: typical MRI appearances and pearls for differential diagnosis. *Quant Imaging Med Surg* **9**, 1966-1972 (2019). https://doi.org:10.21037/qims.2019.08.12

50 Sabanathan, S. *et al.* Expanding the phenotype of children presenting with hypoventilation with biallelic TBCK pathogenic variants and literature review. *Neuromuscul Disord* **33**, 50-57 (2023). https://doi.org:10.1016/j.nmd.2022.10.004

51 Shah, S. N., Gibbs, S., Upton, C. J., Pickworth, F. E. & Garioch, J. J. Incontinentia pigmenti associated with cerebral palsy and cerebral leukomalacia: a case report and

literature review. *Pediatr Dermatol* **20**, 491-494 (2003). https://doi.org:10.1111/j.1525-1470.2003.20607.x

52 Schaefer, G. B., Bodensteiner, J. B., Buehler, B. A., Lin, A. & Cole, T. R. The neuroimaging findings in Sotos syndrome. *Am J Med Genet* **68**, 462-465 (1997). https://doi.org:10.1002/(sici)1096-8628(19970211)68:4<462::aid-ajmg18>3.0.co;2-q

53 Ah Mew, N. *et al.* MRI features of 4 female patients with pyruvate dehydrogenase E1 alpha deficiency. *Pediatr Neurol* **45**, 57-59 (2011). https://doi.org:10.1016/j.pediatrneurol.2011.02.003

54 Riva, A. *et al.* A Phenotypic-Driven Approach for the Diagnosis of WOREE Syndrome. *Front Pediatr* **10**, 847549 (2022). https://doi.org:10.3389/fped.2022.847549

55 Maroofian, R. *et al.* Homozygous missense WIPI2 variants cause a congenital disorder of autophagy with neurodevelopmental impairments of variable clinical severity and disease course. *Brain Commun* **3**, fcab183 (2021). https://doi.org:10.1093/braincomms/fcab183

56 Richard, E. M. *et al.* Bi-allelic variants in SPATA5L1 lead to intellectual disability, spastic-dystonic cerebral palsy, epilepsy, and hearing loss. *Am J Hum Genet* **108**, 2006-2016 (2021). https://doi.org:10.1016/j.ajhg.2021.08.003

57 Grange, D. K. *et al.* Cantu syndrome: Findings from 74 patients in the International Cantu Syndrome Registry. *Am J Med Genet C Semin Med Genet* **181**, 658-681 (2019). https://doi.org:10.1002/ajmg.c.31753

58 Harakalova, M. *et al.* Dominant missense mutations in ABCC9 cause Cantu syndrome. *Nat Genet* **44**, 793-796 (2012). https://doi.org:10.1038/ng.2324

59 Roessler, H. I. *et al.* Three-dimensional facial morphology in Cantu syndrome. *Am J Med Genet A* **182**, 1041-1052 (2020). https://doi.org:10.1002/ajmg.a.61517

60 McClenaghan, C. *et al.* Skeletal muscle delimited myopathy and verapamil toxicity in SUR2 mutant mouse models of AIMS. *EMBO Mol Med*, e16883 (2023). https://doi.org:10.15252/emmm.202216883

61 Yamada, K. *et al.* Protective role of ATP-sensitive potassium channels in hypoxia-induced generalized seizure. *Science* **292**, 1543-1546 (2001). https://doi.org:10.1126/science.1059829

62 Gimenez-Cassina, A. *et al.* BAD-dependent regulation of fuel metabolism and K(ATP) channel activity confers resistance to epileptic seizures. *Neuron* **74**, 719-730 (2012). https://doi.org:10.1016/j.neuron.2012.03.032

63 Martinez-Francois, J. R. *et al.* BAD and K(ATP) channels regulate neuron excitability and epileptiform activity. *Elife* **7** (2018). https://doi.org:10.7554/eLife.32721

64 Sun, H. S. & Feng, Z. P. Neuroprotective role of ATP-sensitive potassium channels in cerebral ischemia. *Acta Pharmacol Sin* **34**, 24-32 (2013). https://doi.org:10.1038/aps.2012.138

65 Liss, B. & Roeper, J. Molecular physiology of neuronal K-ATP channels (review). *Mol Membr Biol* **18**, 117-127 (2001).

66 Pocai, A. *et al.* Hypothalamic K(ATP) channels control hepatic glucose production. *Nature* **434**, 1026-1031 (2005). https://doi.org:10.1038/nature03439

67 Karlsson, M. *et al.* A single-cell type transcriptomics map of human tissues. *Sci Adv* **7** (2021). https://doi.org:10.1126/sciadv.abh2169

68 Nelson, P. T. *et al.* ABCC9 gene polymorphism is associated with hippocampal sclerosis of aging pathology. *Acta Neuropathol* **127**, 825-843 (2014). https://doi.org:10.1007/s00401-014-1282-2

69 Hariharan, A., Robertson, C. D., Garcia, D. C. G. & Longden, T. A. Brain capillary pericytes are metabolic sentinels that control blood flow through a K(ATP) channel-dependent energy switch. *Cell Rep* **41**, 111872 (2022). https://doi.org:10.1016/j.celrep.2022.111872

70 Proks, P. *et al.* Molecular basis of Kir6.2 mutations associated with neonatal diabetes or neonatal diabetes plus neurological features. *Proc Natl Acad Sci U S A* **101**, 17539-17544 (2004). https://doi.org:10.1073/pnas.0404756101

71 Proks, P. *et al.* A heterozygous activating mutation in the sulphonylurea receptor SUR1 (ABCC8) causes neonatal diabetes. *Hum Mol Genet* **15**, 1793-1800 (2006). https://doi.org:10.1093/hmg/ddl101

72 Gloyn, A. L. *et al.* Activating mutations in the gene encoding the ATP-sensitive potassium-channel subunit Kir6.2 and permanent neonatal diabetes. *N Engl J Med* **350**, 1838-1849 (2004). https://doi.org:10.1056/NEJMoa032922

73 D'Adamo, M. C., Catacuzzeno, L., Di Giovanni, G., Franciolini, F. & Pessia, M. K(+) channelepsy: progress in the neurobiology of potassium channels and epilepsy. *Front Cell Neurosci* **7**, 134 (2013). https://doi.org:10.3389/fncel.2013.00134

Figure legends

Figure 1 Clinical features and neuroradiological phenotype of *ABCC9* patients. (A) Clinical photographs. Patient 1-1 at age 30 exhibits hypotelorism, broad nasal tip and large frontal incisors. Patients 2-1 and 2-2 show a variable association of cognitive impairment and spasticity, with a more severe involvement and decerebrate posture in 2-1. Subject 5-1 shows microcephaly, hypotonia, spasticity, drooling, and kyphosis. She also has dysmorphic features consisting of bossing forehead, sparse thin hair, epicanthic folds, prominent nose, retrognathia, and low set ears. Subject 6-1 at age 13 shows synophrys, anteverted nostrils, thin upper lip and small chin. Epidermal scar-like nevus left cheek. (**B)** Neuroimaging findings of patients compared with a normal control. Brain MRI studies with sagittal T1-weighted (first images), axial T2 or FLAIR (second and third images) and coronal T2 or FLAIR images (last images) performed in Patient 1-1 at 15 years of age, Patient 3-1 at 9 months of age, Patient 5-1 at 10 months of age, Patient 6-1 at 7 years of age, and Patient 6-2 at 1 years and 8 months of age. Head CT, axial images, performed in Patients 3-1 and 6-1 at 6 months and 7 years, respectively. There is reduction of parieto-occipital white matter volume with T2/FLAIR hyperintensities and squared-appearance of the lateral ventricles in all subjects (empty arrows). The signal abnormalities extend to the frontal lobes in Patients 1-1, 5-1, 6-1 and 6-2 (arrowheads) and to the anterior temporal regions in Patients 1-1 and 5-1 (thick arrows). Note the small cavitations in the frontal regions in Patient 1-1 and the involvement of the anterior portions of the external capsules (dashed arrows) in

Patients 1-1 and 5-1. The corpus callosum is thin in Patients 1-1, 3-1 and 5-1 (curved arrows). Axial CT images reveal multiple small calcifications at the level of the frontal periventricular white matter and right putamen in Patient 3-1 and at the level of the fronto-parietal white matter and cortex in Patient 6-1 (thin arrows).

Figure 2 Molecular consequences of *ABCC9* variants in AIMS individuals. (A) Agarose gel electrophoresis of RT-PCR products showing amplicons from cells transfected with pSPL3 minigene vectors containing either the *ABCC9* c.284+1A or c.4212-1T variant, wild-type *ABCC9* sequences or the pSPL3 vector alone with no *ABCC9* insertion. **(B)** Schematic representation of the mini-gene construct (*top right*). Exon 2 or 35 of *ABCC9* with the flanking 5' and 3' intronic regions was inserted between exon A and exon B of the pSPL3 vector. Sanger sequencing of the RT-PCR amplicons revealed that the c.284+1A variant results in skipping of exon 2 and the c.4212-1T variant resulted in activation of a cryptic splice site resulting in exclusion of 11 bases from exon 37 and the predicted p.(Phe1405SerfsTer8) frameshift. Canonical splicing of WT *ABCC9*-containing vector resulted in inclusion of full-length exon 2 or 35. RT-PCR from cells transfected with the empty pSPL3 vector (i.e. no *ABCC9* sequence inserted) resulted in the expected amplification of the pSPL3 exons A and B only. **(C)** K_{ATP} channels assemble as octameric complexes with 4 Kir6 subunits (black) and 4 SUR subunits (grey). SUR subunits comprise 17 transmembrane domains in three domains (TMD0, TMD1, and TMD2) and two intracellular nucleotide binding domains (NBD1 and NBD2). All variants identified in affected AIMS individuals are predicted or shown to result in splicing defects and major in-frame deletion, or in premature stop codons. Family pedigrees shown for each case, arrow denotes proband.

Figure 3 AIMS associated mutations cause complete K_{ATP} channel loss-of-function. (A) Whole-cell patch clamp recordings were performed in HEK293 cells transfected with Kir6.2 and WT or mutant SUR2A. Initial ambient levels of intracellular ATP means channels are inhibited immediately after membrane rupture to whole-cell configuration. Over time, ATP levels are depleted by dilution with the pipette solution. **(B)** Example current traces from voltage ramps for cells transfected with GFP alone, or Kir6.2 alongside SUR2A-WT, SUR2[Arg620Ter],

SUR2[Arg938Ter], SUR2[Phe1405SerfsTer8], or SUR2[Leu714SerfsTer7]. **(C)** Summary showing whole-cell currents at 0 mV measured at 10 minutes after establishing the whole-cell recording configuration. Box and Whisker plot shows median as horizontal line, mean as X, and interquartile range as colored box. *P* values from Dunn's pairwise comparisons versus SUR2A-WT following Kruskal-Wallis test shown. **(D)** K_{ATP} currents were recorded from cells transfected with Kir6.2 and SUR2A-WT (top, grey) or SUR2[Phe1405SerfsTer8] (bottom, orange). Whole cell currents were recorded from ramp protocols as shown above with 300 µM ATP included in the patch pipette. Currents at 0 mV from sweeps recorded at 5 sec intervals are shown. K_{ATP} channels from SUR2A-WT expressing cells displayed robust activation upon administration of 100 µM pinacidil, which was reversed by the K_{ATP} inhibitor glibenclamide (10 µM). Dotted line shows zero current level. (**E**) Summary of currents recorded prior to- and after pinacidil administration in cells transfected with Kir6.2 and SUR2A-WT or SUR2[Phe1405SerfsTer8]. *P* values from Dunn's pairwise comparisons versus SUR2A-WT currents in pinacidil following Kruskal-Wallis test shown.

Figure 4 SUR2-STOP zebrafish larvae exhibit increased seizure susceptibility and dysmorphology. (A) Automated swim tracking was used to measure motility in LoF SUR2-STOP fish and WT controls. Swimming distances prior to pentylenetetrazole (PTZ; 3 mM) administration (-) and after PTZ (+) shown. Data from individual measurements from biological replicates as dots with mean and S.E.M. shown. Measurements were made and combined from 3 separate breeding clutches. *** denotes $p < 0.001$ and **** denotes $p < 0.0001$ from Tukey tests following one-way ANOVA. **(B)** Swimming distance for each larva after PTZ administration was normalized to basal activity prior to PTZ. Data from individual measurements from biological replicates shown as dots with mean and S.E.M. shown. **** denotes $p < 0.0001$ according to unpaired t-test. **(C)** Plot showing the cumulative distance swam for WT and SUR2-STOP larvae after PTZ administration. Swimming distances are normalized to the average swimming distances for each genotype over 30 s prior to PTZ admin. Data shown as mean (solid line) and S.E.M. as shaded bars. **(D-H)** Morphometric analysis of WT and SUR2-STOP larvae showing reduced body length **(D)**, equivalent head dimensions **(E-F)**, and reduced inter-eye and eye diameter measurements **(G-H)** in SUR2-STOP larvae. Data from individual measurements

from biological replicates as dots with mean and S.E.M. shown. ** denotes $p < 0.01$ and **** denotes $p < 0.0001$ according to unpaired t-tests.

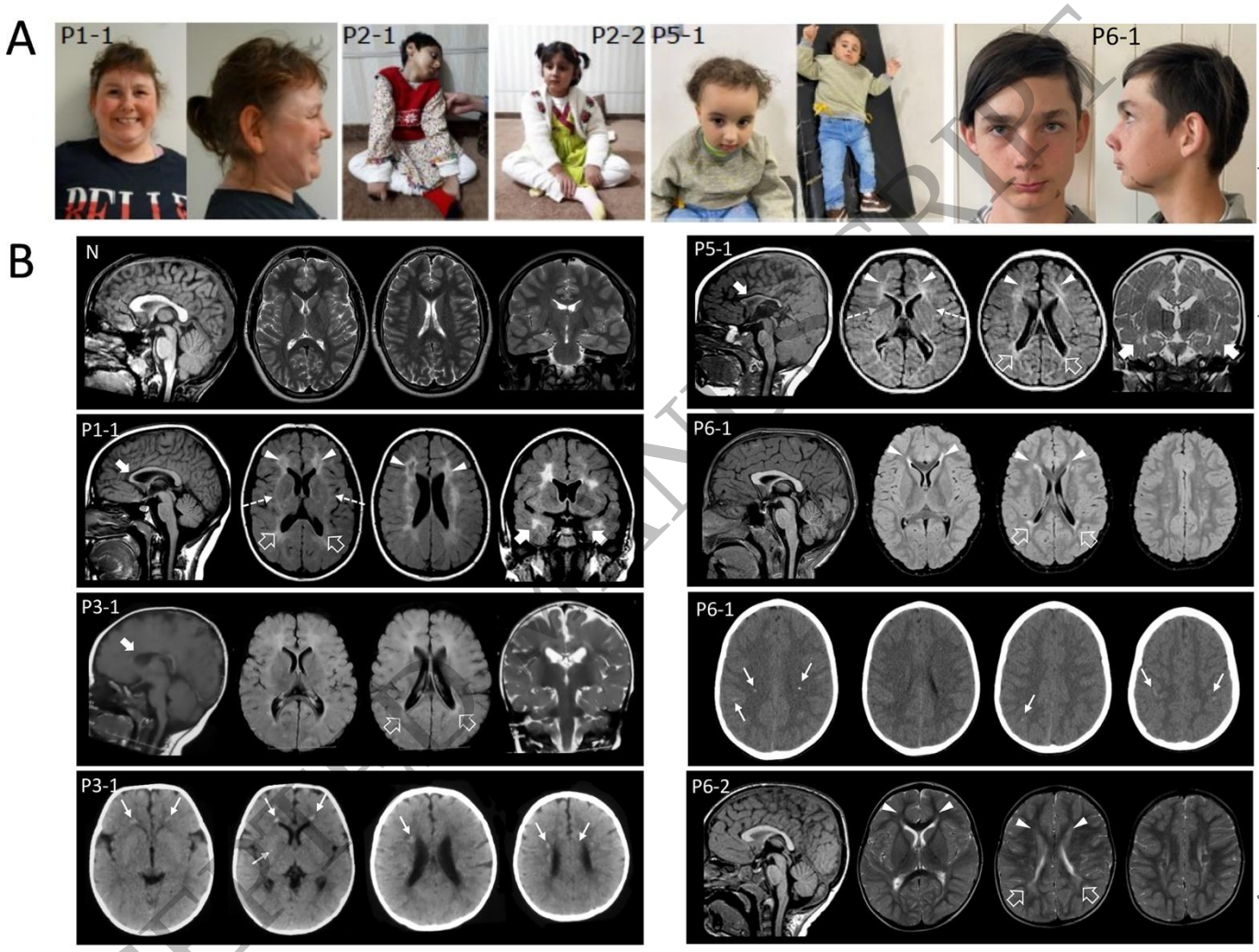

Figure 1
185x142 mm (x DPI)

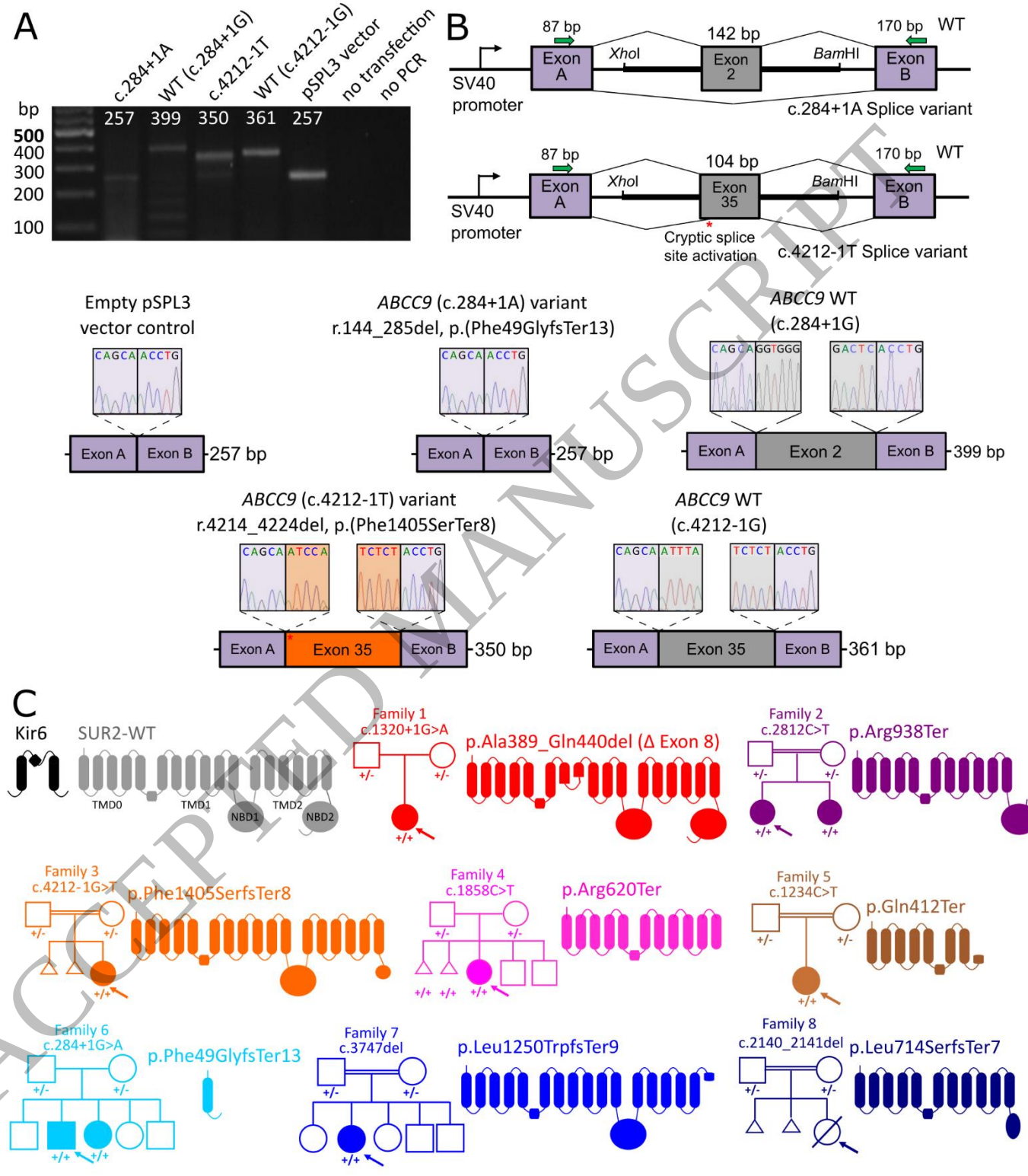

Figure 2
186x210 mm (x DPI)

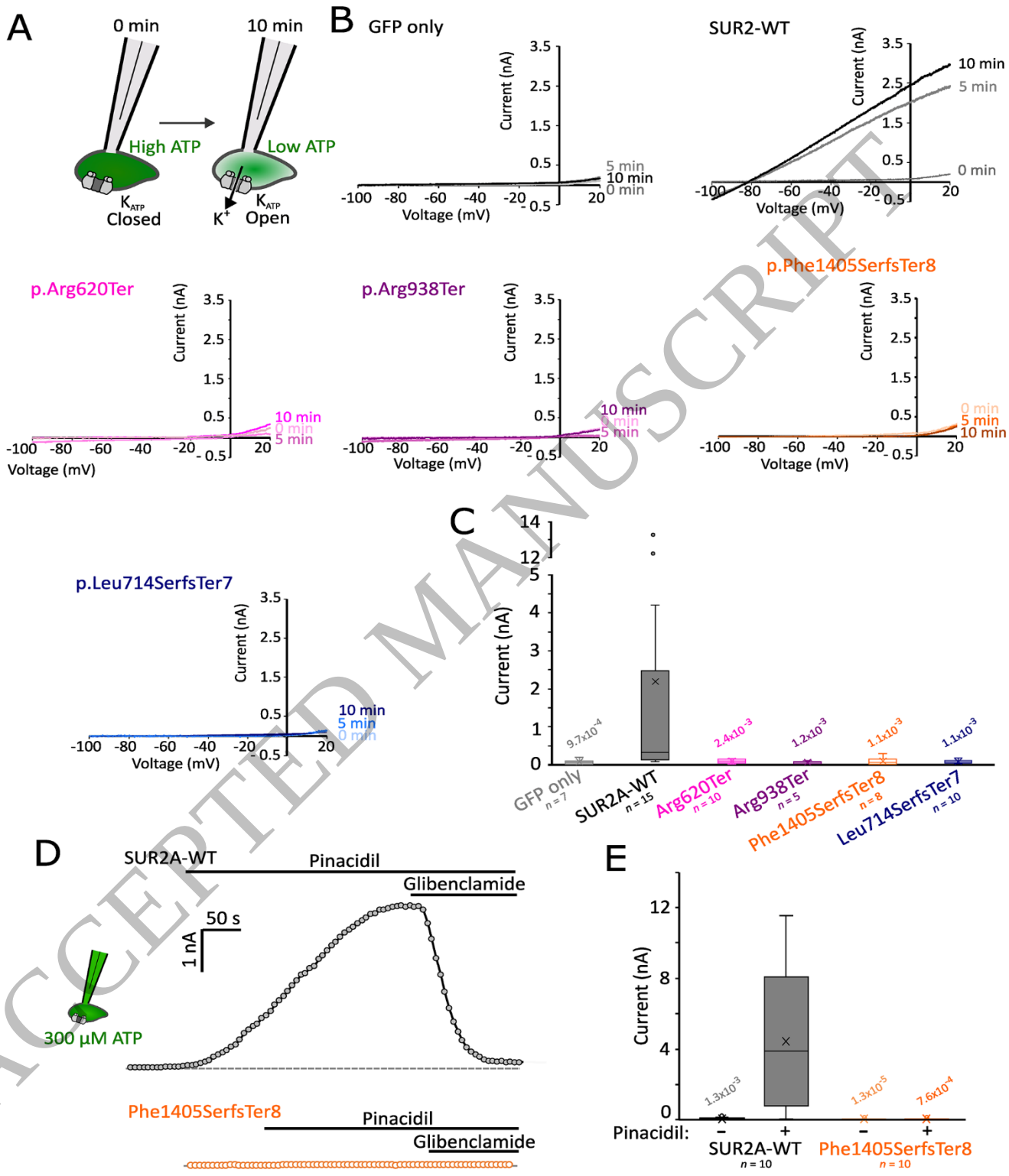

Figure 3
185x222 mm (x DPI)

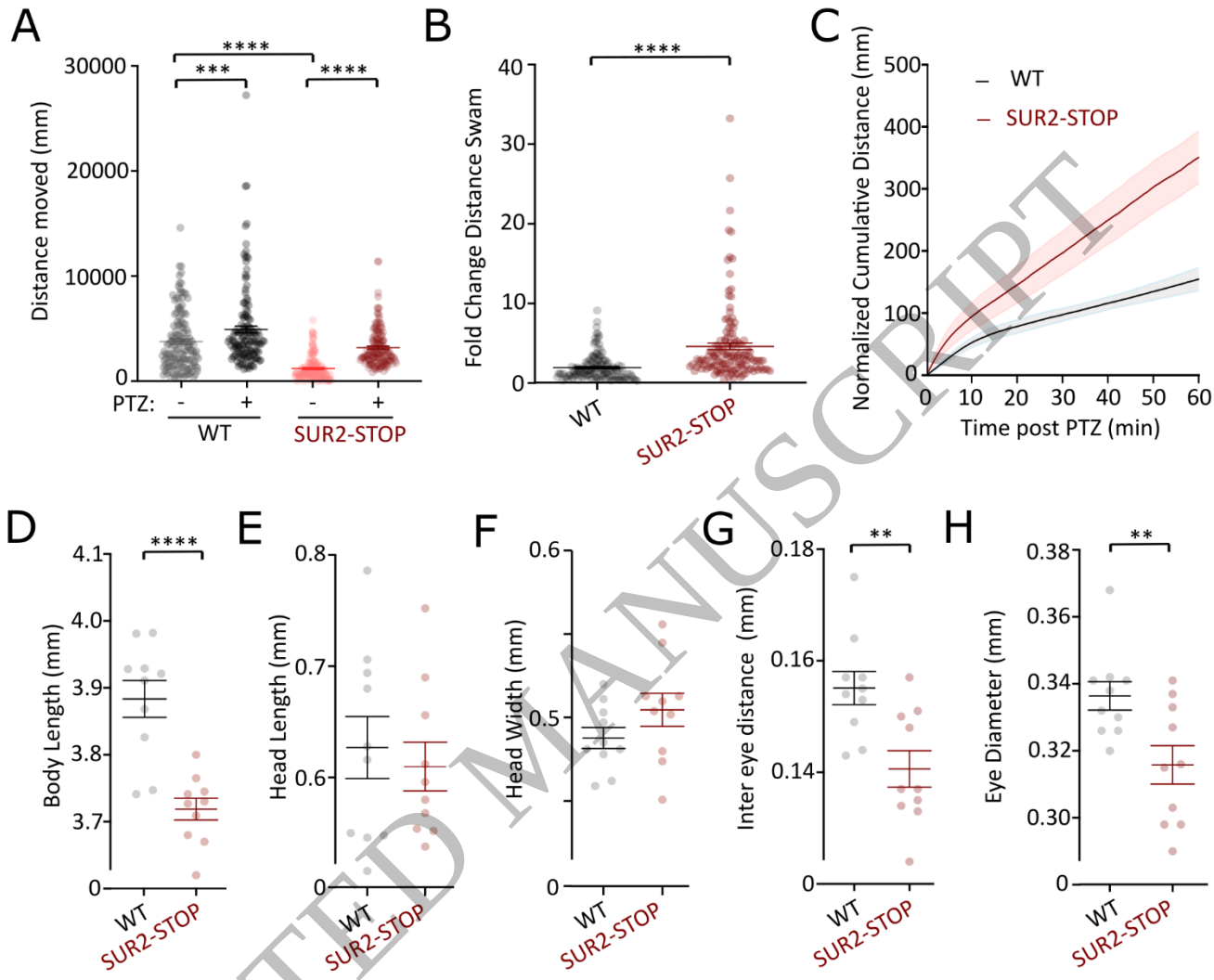

Figure 4
179x145 mm (x DPI)

Table 1 Demographic, genetic, and key clinical features of AIMS patients

Patient ID	**1-1**	**2-1**	**2-2**	**3-1**	**4-1**	**5-1**	**6-1**	**6-2**	**7-1**
Family ID	**F1**	**F2**	**F2**	**F3**	**F4**	**F5**	**F6**	**F6**	**F7**
Demographics									
Age	31 y	7.5 y	10.5 y	4.5 y	14 y	4 y	13 y	10 y	36 y
Sex	F	F	F	F	F	F	M	F	F
Nationality	Norwegian	Pakistani	Pakistani	Egyptian	Dutch	Egyptian	Norwegian	Norwegian	British Pakistani
Genetics									
gDNA (hg38)	chr12-21910156-C-T	chr12-21848204-G-A	chr12-21848204-G-A	chr12-21809956-C-A	chr12-21887879-G-A	chr12-21910243-G-A	chr12-21910243-G-A	chr12-21910243-G-A	chr12-21818174del
cDNA[a]	c.1320+1G>A	c.2812C>T	c.2812C>T	c.4212-1G>T	c.1858C>T	c.1234C>T	c.284+1G>A	c.284+1G>A	c.3747del
Protein	p.(Ala389_Gln440del)	p.(Arg938Ter)	p.(Arg938Ter)	p.(Phe1405SerfsTer8)	p.(Arg620Ter)	p.(Gln412Ter)	p.(Phe49GlyfsTer13)	p.(Phe49GlyfsTer13)	p.(Leu1250TrpfsTer9)
Consanguinity	No	Yes	Yes	Yes	No	Yes	No	No	Yes
Select Clinical Features									
Developmental Delay	Global	Global	Global	Motor	Global, mild	Global	Mild DD	Mild DD	Global
Intellectual disability	Severe	Severe	Severe	No	Mild	Mild	Mild	Learning difficulties	Mild learning disability
Microcephaly	No	Yes	Yes	Yes	No	Yes	Yes	No	Yes
Spasticity	Yes	Yes	Yes	Yes	No	Yes	Yes	Yes	No
Seizures	Yes	Yes	No	No	Yes	No	Yes	No	No
Fatigability	Yes	NA	NA	Yes	Yes	Yes	Yes	Yes	Yes
White matter signal alterations	Yes	No	No	Yes	No	Yes	Yes	Yes	NA

NA = not assessed.
[a]NM_005691.

Table 2 Summary of the cardinal clinical features in AIMS patients

Clinical features	**Our cohort (n = 9)**	**%**	**Previous AIMS patients[1] (n = 6)**	**%**	**Total (n = 15)**	**%**
Developmental Delay	9	100	6	100	15	100
Intellectual disability	8	89	6	100	14	93
Fatigability	7	78	6	100	13	87
White matter signal alterations	5	56	6	100	11	73
Lordosis/Scoliosis	5	56	5	83	10	67
Dysmorphism	4	44	6	100	10	67
Neuropsychiatric manifestations	5	56	4	67	9	60
Contractures	5	56	4	67	9	60
Microcephaly	6	67	2	33	8	53
Corpus callosum hypoplasia/agenesis	6	67	0	0	6	40
Seizures	4	44	1	17	5	33
Cardiac abnormalities	1	11	2	33	3	20
Other MRI abnormalities	2	22	0	0	2	13